

# Bifunctional Compounds for Controlling Metal-Mediated Aggregation of the $A\beta_{42}$ Peptide

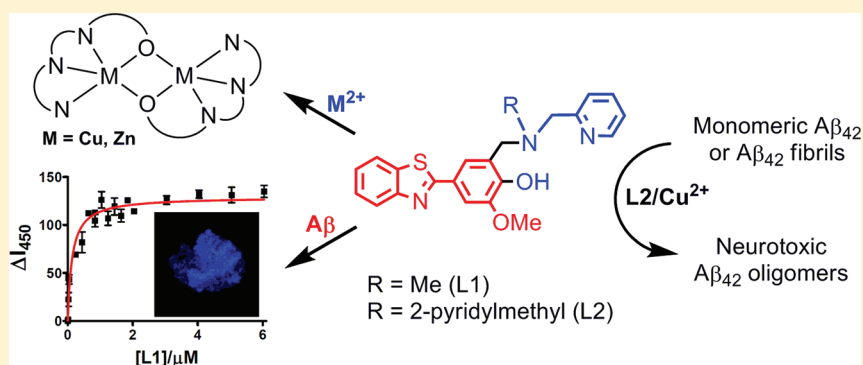
Anuj K. Sharma,<sup>†</sup> Stephanie T. Pavlova,<sup>†</sup> Jaekwang Kim,<sup>‡</sup> Darren Finkelstein,<sup>†</sup> Nicholas J. Hawco,<sup>†</sup> Nigam P. Rath,<sup>§</sup> Jungsu Kim,<sup>‡</sup> and Liviu M. Mirica<sup>\*†</sup>

<sup>†</sup>Department of Chemistry, Washington University, One Brookings Drive, St. Louis, Missouri 63130-4899, United States

<sup>‡</sup>Department of Neurology, Washington University School of Medicine, St. Louis, Missouri 63108, United States

<sup>§</sup>Department of Chemistry and Biochemistry, University of Missouri St. Louis, One University Boulevard, St. Louis, Missouri 63121-4400, United States

## Supporting Information



**ABSTRACT:** Abnormal interactions of Cu and Zn ions with the amyloid  $\beta$  ( $A\beta$ ) peptide are proposed to play an important role in the pathogenesis of Alzheimer's disease (AD). Disruption of these metal–peptide interactions using chemical agents holds considerable promise as a therapeutic strategy to combat this incurable disease. Reported herein are two bifunctional compounds (BFCs) L1 and L2 that contain both amyloid-binding and metal-chelating molecular motifs. Both L1 and L2 exhibit high stability constants for  $Cu^{2+}$  and  $Zn^{2+}$  and thus are good chelators for these metal ions. In addition, L1 and L2 show strong affinity toward  $A\beta$  species. Both compounds are efficient inhibitors of the metal-mediated aggregation of the  $A\beta_{42}$  peptide and promote disaggregation of amyloid fibrils, as observed by ThT fluorescence, native gel electrophoresis/Western blotting, and transmission electron microscopy (TEM). Interestingly, the formation of soluble  $A\beta_{42}$  oligomers in the presence of metal ions and BFCs leads to an increased cellular toxicity. These results suggest that for the  $A\beta_{42}$  peptide—in contrast to the  $A\beta_{40}$  peptide—the previously employed strategy of inhibiting  $A\beta$  aggregation and promoting amyloid fibril disaggregation may not be optimal for the development of potential AD therapeutics, due to formation of neurotoxic soluble  $A\beta_{42}$  oligomers.

## INTRODUCTION

Alzheimer's disease (AD) is the most common cause of age-related senile dementia, as more than 5 million in the US and 24 million people worldwide suffer from this neurodegenerative disease.<sup>1–3</sup> To date there is no treatment for AD and its diagnosis with high accuracy requires a detailed post-mortem examination of the brain.<sup>4</sup> The brains of AD patients are characterized by the deposition of amyloid plaques whose main component is the amyloid  $\beta$  ( $A\beta$ ) peptide.<sup>5</sup> The main alloforms of the  $A\beta$  peptide are 42 and 40 amino acids long ( $A\beta_{42}$  and  $A\beta_{40}$ , respectively);<sup>6,7</sup>  $A\beta_{40}$  is present in larger amounts in the brain, yet  $A\beta_{42}$  is more neurotoxic and has a higher tendency to aggregate.<sup>8–11</sup> According to the amyloid cascade hypothesis, the increased production and accumulation of the  $A\beta$  peptide promote the formation of  $A\beta$  oligomers, protofibrils, and ultimately amyloid fibrils that lead to neurodegeneration.<sup>12,13</sup> However, recent *in vivo* studies have shown that the soluble  $A\beta$

oligomers are possibly more neurotoxic than amyloid plaques<sup>14–17</sup> and are likely responsible for synaptic dysfunction and memory loss in AD patients and AD animal models.<sup>18–21</sup> In this regard, efforts to rationally design AD therapeutics based on compounds that control  $A\beta$  aggregation have been hampered by the lack of a complete understanding of the neurotoxic role of various  $A\beta$  aggregates.<sup>22</sup>

Remarkably high concentrations of Zn, Cu, and Fe have been found within the amyloid deposits in AD-affected brains,<sup>23,24</sup> and several studies have investigated the interactions of metal ions with monomeric  $A\beta$  peptides and their correlation with amyloid plaque formation.<sup>23–29</sup> Thus, these metal ions have been shown to promote  $A\beta_{40}$  aggregation,<sup>23–27,29–32</sup> as well lead to formation of reactive oxygen species (ROS) and

Received: November 10, 2011

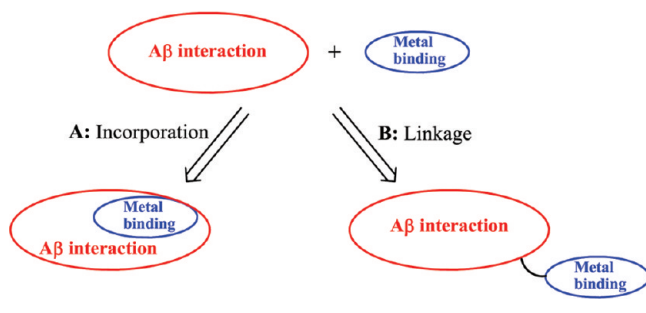
Published: March 27, 2012

oxidative stress.<sup>3,26–31,33–36</sup> However, the role of metal ions in  $A\beta_{42}$  aggregation still remains unclear and only few reports are available in the literature.<sup>37–41</sup> For example, while  $Zn^{2+}$  was shown to cause rapid formation of nonfibrillar aggregates,<sup>41</sup>  $Cu^{2+}$  was shown to reduce  $A\beta_{42}$  aggregation.<sup>39,40</sup> Overall, these studies confirm that metal ions modulate the various pathways of  $A\beta$  aggregation and toxicity,<sup>42</sup> yet the molecular mechanisms of metal– $A\beta$  species interactions, especially for the more neurotoxic  $A\beta_{42}$ , are not completely understood.

Given the recognized interactions of  $A\beta$  with transition metal ions, several studies have shown that metal chelators can reduce the metal-mediated  $A\beta$  aggregation, ROS formation, and neurotoxicity *in vitro*.<sup>43–45</sup> For example, the nonspecific chelator clioquinol (CQ) showed decreased  $A\beta$  aggregate formation that resulted in improved cognition in clinical trials.<sup>24,25,43–45</sup> However, use of nonspecific chelators (i.e., CQ) that do not interact selectively with the  $A\beta$ –metal species exhibit adverse side effects that will likely limit their long-term clinical use.<sup>3,28,29,31,44,46–48</sup>

Recent efforts in studying the  $A\beta$ –metal interactions have focused on small molecules, bifunctional chelators (BFCs), which can interact with the  $A\beta$  peptide and also bind the metal ions from the  $A\beta$ –metal species. Such bifunctional compounds should potentially lead to more effective therapeutic agents, as well as provide an increased understanding of the metal– $A\beta$  associated neuropathology. In this context, two approaches have been pursued in BFC design.<sup>31,49–58</sup> One strategy is based on the direct incorporation of metal-binding atom donors into the structural framework of an  $A\beta$ -interacting compound (Scheme 1, approach A), and the other involves linking the

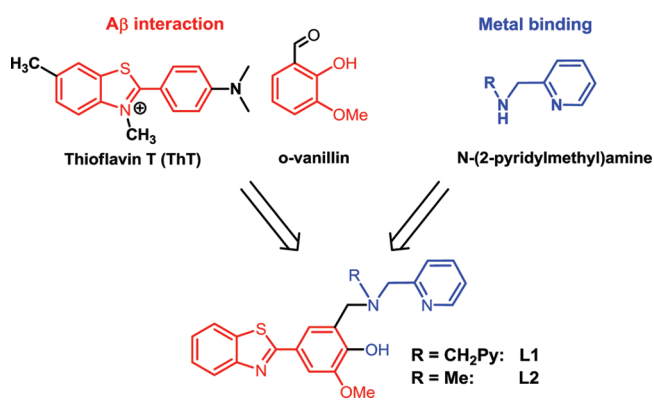
**Scheme 1. Pictorial Representation of the Two Approaches Employed in Bifunctional Chelator Design**



metal-chelating and  $A\beta$ -binding molecular fragments (Scheme 1, approach B). While the former approach has recently been employed in several classes of compounds,<sup>51,52,57,59</sup> only a few examples have been designed based on the latter approach.<sup>49,53,54</sup>

Reported herein are two new BFCs, L1 and L2, that were designed following the linkage approach and contain metal-binding *N*-(2-pyridylmethyl)amine groups and amyloid-interacting 2-phenylbenzothiazole and *o*-vanillin molecular fragments (Scheme 2).<sup>59</sup> The bifunctional character of the two compounds was confirmed by metal-chelating and  $A\beta$ -binding studies that reveal a tight binding to  $Cu$  and  $Zn$  ions and high affinity for the  $A\beta$  fibrils. The  $A\beta$ -binding ability of the two bifunctional compounds was determined by taking advantage of their intrinsic fluorescence properties. L1 and L2 are, to the best of our knowledge, the first bifunctional chelators for which  $A\beta$  fibril binding affinities were measured. In addition, the corresponding  $Cu^{2+}$  and  $Zn^{2+}$  complexes were isolated and

**Scheme 2. Employed Synthetic Strategy for Bifunctional Chelators**



characterized structurally and spectroscopically. These BFCs were also able to inhibit the metal-mediated  $A\beta$  aggregation and disassemble preformed  $A\beta$  aggregates. Most notably, this is the first detailed study of the interaction of bifunctional compounds with the more aggregation-prone  $A\beta_{42}$  peptide, which is proposed to be physiologically relevant due to the formation of  $A\beta_{42}$  oligomers.<sup>10,11,18–20</sup> Intriguingly, the ability of the developed BFCs to inhibit  $A\beta$  fibril formation and promote fibril disaggregation leads to increased cellular toxicity. This suggests that the previously proposed strategy of limiting  $A\beta$  aggregation may not be optimal for the  $A\beta_{42}$  peptide as it may generate neurotoxic soluble  $A\beta_{42}$  oligomers. As such, future bifunctional chelator design approaches should be aimed at controlling these soluble  $A\beta_{42}$  oligomers.

## EXPERIMENTAL SECTION

**General Methods.** All reagents were purchased from commercial sources and used as received unless stated otherwise. Solvents were purified prior to use by passing through a column of activated alumina using an MBRAUN SPS. All solutions and buffers were prepared using metal-free Millipore water that was treated with Chelex overnight and filtered through a 0.22  $\mu$ m nylon filter.  $^1H$  (300.121 MHz) and  $^{13}C$  (151 MHz) NMR spectra were recorded on a Varian Mercury-300 spectrometer. Chemical shifts are reported in ppm and referenced to residual solvent resonance peaks. UV–visible spectra were recorded on a Varian Cary 50 Bio spectrophotometer and are reported as  $\lambda_{max}$  nm ( $\epsilon$ ,  $M^{-1} cm^{-1}$ ). ESI-MS experiments were performed using a Bruker Maxis QTOF mass spectrometer with an electrospray ionization source. Solution magnetic susceptibility measurements were obtained by the Evans method<sup>60</sup> using coaxial NMR tubes and  $CD_3CN$  or  $CD_2Cl_2$  as a solvent at 298 K; diamagnetic corrections were estimated using Pascal's constants.<sup>61</sup> ESI mass-spectrometry was provided by the Washington University Mass Spectrometry NIH Resource (Grant no. P41RR0954), and elemental analyses were carried out by the Columbia Analytical Services Tucson Laboratory. TEM analysis was performed at the Nano Research Facility (NRF) at Washington University.

**Syntheses.** **L1.** Paraformaldehyde (0.296 g, 9.86 mmol) was added to a solution of bis-(2-picolyl)amine (1.798 g, 9.02 mmol) in EtOH (75 mL) and the resultant mixture was heated to reflux for 1 h. Then 2-(4-hydroxy-3-methoxy)-benzothiazole<sup>62</sup> (2.113 g, 8.99 mmol) in EtOH (70 mL) was added, the solution was refluxed for an additional 48 h, and then cooled to room temperature. The solvent was removed to give a light yellow residue that was purified by silica gel column chromatography using EtOAc/*i*PrOH/ $NH_4OH$  (75:20:5) to yield a white solid (2.98 g, yield 71%).  $^1H$  NMR ( $CDCl_3$ ):  $\delta$  8.56 (d, 2H, PyH), 8.01 (d, 1H, ArH), 7.87 (d, 1H, ArH), 7.60–7.66 (m, 3H, ArH), 7.43–7.49 (m, 1H, ArH), 7.31–7.38

(m, 3H, PyH and phenol H), 7.15–7.19 (m, 2H, PyH and PyH3), 4.05 (s, 3H, OCH<sub>3</sub>), 3.93 (s, 4H, NCH<sub>2</sub>Py), 3.89 (s, 2H, CH<sub>2</sub>N). <sup>13</sup>C NMR (CDCl<sub>3</sub>): δ 168.5, 158.3, 154.4, 150.4, 149.1, 149.0, 137.1, 135.0, 126.3, 124.8, 124.4, 123.8, 122.8, 122.6, 122.6, 122.4, 121.6, 110.1, 59.1, 56.7, 56.3. UV–vis, MeCN, λ<sub>max</sub> nm (ε, M<sup>-1</sup> cm<sup>-1</sup>): 226 (35800), 330 (25800). HR-MS: Calcd for [M + H]<sup>+</sup>, 469.1698; found, 469.1689.

L2. Paraformaldehyde (0.086 g, 2.86 mmol) was added to a solution of *N*-Methyl-2-pyridinemethanamine (0.235 g, 1.925 mmol) in EtOH (5 mL) and the resultant mixture was heated to reflux for 1 h. A hot solution of 2-(4-hydroxy-3-methoxy)benzothiazole (0.5 g, 1.923 mmol) in EtOH (10 mL) was added to the reaction flask and the solution was refluxed for an additional 24 h. The solvent was removed and the resulting residue was purified by silica gel column chromatography using EtOAc/Hexane (1:1) to yield a white solid (0.510 g, yield 67%). <sup>1</sup>H NMR (CDCl<sub>3</sub>): δ 8.61 (d, 1H, Py2H), 8.01 (d, 1H, ArH), 7.87 (d, 1H, ArH), 7.69 (dt, 1H, PyH4), 7.59 (d, 1H, ArH), 7.47 (t, 1H, ArH), 7.33–7.37 (m, 3H, ArH and PyH3), 7.32 (s, 1H, ArH), 7.22 (t, 1H, PyH5), 4.03 (s, 3H, OCH<sub>3</sub>), 3.88 (s, 4H, CH<sub>2</sub>NCH<sub>2</sub>), 2.37 (s, 3H, NCH<sub>3</sub>). <sup>13</sup>C NMR (CDCl<sub>3</sub>): δ 168.4, 157.1, 154.3, 150.5, 149.5, 148.6, 137.1, 134.9, 126.3, 124.8, 124.7, 123.4, 122.8, 122.8, 122.7, 121.6, 121.1, 110.1, 63.0, 60.2, 56.3, 42.0. UV–vis, MeCN, λ<sub>max</sub> nm (ε, M<sup>-1</sup> cm<sup>-1</sup>): 226 (36,300), 348 (25,300). HR-MS: Calcd for [M + H]<sup>+</sup>, 392.1433; found, 392.1426.

[(L1)Cu<sup>II</sup>]<sub>2</sub>(ClO<sub>4</sub>)<sub>2</sub>·H<sub>2</sub>O (1). A solution of [Cu<sup>II</sup>(H<sub>2</sub>O)<sub>6</sub>](ClO<sub>4</sub>)<sub>2</sub> (0.119 g, 0.32 mmol) was added to a stirring solution of L1 (0.15 g, 0.32 mmol) in MeCN (5 mL) and Et<sub>3</sub>N (0.064 g, 0.64 mmol). The brown solution was stirred for 30 min. Addition of Et<sub>2</sub>O resulted in the formation of a brown precipitate which was filtered, washed with Et<sub>2</sub>O, and dried under vacuum (0.209 g, yield 54%). UV–vis, MeCN, λ<sub>max</sub> nm (ε, M<sup>-1</sup> cm<sup>-1</sup>): 226 (63100), 348 (60200), 425 (650), 832 (230). HR-MS: Calcd for [(L1)Cu]<sub>2</sub><sup>2+</sup>, 530.0838; found, 530.0833. Room temperature solution magnetic moment μ<sub>eff</sub> = 1.72 μ<sub>B</sub>/Cu<sup>2+</sup>. Anal. Found: C, 50.22; H, 3.35; N, 9.09. Calcd for C<sub>54</sub>H<sub>46</sub>Cl<sub>2</sub>Cu<sub>2</sub>N<sub>8</sub>O<sub>12</sub>S<sub>2</sub>·H<sub>2</sub>O: C, 50.70; H, 3.78; N, 8.76.

[(L1)Zn<sup>II</sup>]<sub>2</sub>(ClO<sub>4</sub>)<sub>4</sub>·2MeOH·2H<sub>2</sub>O (2). A solution of [Zn<sup>II</sup>(H<sub>2</sub>O)<sub>6</sub>](ClO<sub>4</sub>)<sub>2</sub> (0.040 g, 0.106 mmol) in H<sub>2</sub>O (1 mL) was added to a stirring solution of L1 (0.05 g, 0.106 mmol) and Et<sub>3</sub>N (0.022 g, 0.212 mmol) in MeOH (5 mL). The light-yellow solution was stirred for 30 min, and the white precipitate obtained was filtered, washed with Et<sub>2</sub>O, and dried under vacuum (0.048 g, yield 68%). <sup>1</sup>H NMR (CD<sub>3</sub>CN): δ 8.69 (m, 4H), 8.10–7.97 (m, 6H), 7.87 (m, 4H), 7.64–7.35 (m, 10H), 7.22 (m, 4H), 4.04 (s, 6H, OCH<sub>3</sub>), 3.92 (s, 8H, NCH<sub>2</sub>Py), 3.88 (s, 4H, CH<sub>2</sub>N). UV–vis, MeCN, λ<sub>max</sub> nm (ε, M<sup>-1</sup> cm<sup>-1</sup>): 226 (19300), 340 (17900). HR-MS: Calcd for [(L1)Zn]<sub>2</sub><sup>2+</sup>, 531.0833; found, 531.0829. Anal. Found: C, 49.13; H, 4.92; N, 8.59. Calcd for C<sub>54</sub>H<sub>46</sub>Cl<sub>2</sub>N<sub>8</sub>O<sub>12</sub>S<sub>2</sub>Zn<sub>2</sub>·2MeOH·2H<sub>2</sub>O: C, 49.28; H, 4.28; N, 8.21.

[(L2)<sub>2</sub>Cu<sup>II</sup>]<sub>2</sub>(ClO<sub>4</sub>)<sub>2</sub>·H<sub>2</sub>O (3). A solution of [Cu<sup>II</sup>(H<sub>2</sub>O)<sub>6</sub>](ClO<sub>4</sub>)<sub>2</sub> (0.057 g, 0.153 mmol) in MeCN (1 mL) was added to a stirring solution of L2 (0.06 g, 0.153 mmol) and Et<sub>3</sub>N (0.031 g, 0.306 mmol) in MeCN (5 mL). The resulting dark brown solution was stirred for 30 min. Addition of Et<sub>2</sub>O resulted in the formation of a dark brown precipitate which was filtered, washed with Et<sub>2</sub>O, and dried under vacuum (0.040 g, yield 46%). UV–vis, CH<sub>2</sub>Cl<sub>2</sub>, λ<sub>max</sub> nm (ε, M<sup>-1</sup> cm<sup>-1</sup>): 370 (43100), 430 (13700), 520 (1700), 660 (220). HRMS: Calcd for [(L2)Cu]<sub>2</sub><sup>+</sup>, 453.0571; found, 453.0572. Room temperature solution magnetic moment μ<sub>eff</sub> = 1.73 μ<sub>B</sub>/Cu<sup>2+</sup>. Anal. Found: C, 62.21; H, 4.34; N, 9.66. Calcd for C<sub>44</sub>H<sub>40</sub>Cu<sub>2</sub>N<sub>6</sub>O<sub>4</sub>S<sub>2</sub>: C, 62.58; H, 4.77; N, 9.95.

[(L2)<sub>3</sub>Zn<sup>II</sup>]<sub>3</sub>(O)](ClO<sub>4</sub>)<sub>5</sub>·5H<sub>2</sub>O·2MeOH·MeCN (4). A suspension of [Zn<sup>II</sup>(H<sub>2</sub>O)<sub>6</sub>](ClO<sub>4</sub>)<sub>2</sub> (0.076 g, 0.204 mmol) in THF (1 mL) was added to a stirring solution of L2 (0.08 g, 0.204 mmol) and Et<sub>3</sub>N (0.042 g, 0.408 mmol) in THF (5 mL). The yellowish solution was stirred for 30 min. Addition of Et<sub>2</sub>O resulted in the formation of a light yellow precipitate which was filtered, washed with Et<sub>2</sub>O, recrystallized from CH<sub>2</sub>Cl<sub>2</sub>/Et<sub>2</sub>O, and dried under vacuum (0.082 g, yield 70%). <sup>1</sup>H NMR (CDCl<sub>3</sub>): δ 9.04 (d, 1H), 8.44 (d, 1H), 8.16 (d, 1H), 7.95 (d, 2H), 7.88 (d, 2H), 7.75 (s, 1H), 7.60 (t, 1H), 7.48–7.33 (m, 5H), 7.18 (s, 1H), 7.01 (d, 1H), 6.94 (s, 1H), 6.71 (t, 1H), 4.07–3.46 (m, 14H, OCH<sub>3</sub> and CH<sub>2</sub>NCH<sub>2</sub>), 2.85 (s, 3H, NCH<sub>3</sub>), 2.49 (s, 3H, NCH<sub>3</sub>). UV–vis, MeCN, λ<sub>max</sub> nm (ε, M<sup>-1</sup> cm<sup>-1</sup>): 260 (19,200), 348 (15,500).

HR-MS: Calcd for [(L2)Zn]<sub>2</sub><sup>2+</sup>, 454.0568; found, 454.0564. Anal. Found: C, 49.88; H, 5.32; N, 8.10. Calcd for C<sub>66</sub>H<sub>60</sub>ClN<sub>9</sub>O<sub>11</sub>S<sub>3</sub>Zn<sub>3</sub>·5H<sub>2</sub>O·2MeOH·MeCN: C, 50.09; H, 4.86; N, 8.35.

**X-Ray Crystallography.** Suitable crystals of appropriate dimensions were mounted in a Bruker Kappa Apex-II CCD X-Ray diffractometer equipped with an Oxford Cryostream LT device and a fine focus Mo Kα radiation X-Ray source (λ = 0.71073 Å). Preliminary unit cell constants were determined with a set of 36 narrow frame scans. Typical data sets consist of combinations of φ and θ scan frames with a typical scan width of 0.5° and a counting time of 15–30 s/frame at a crystal-to-detector distance of ~4.0 cm. The collected frames were integrated using an orientation matrix determined from the narrow frame scans. Apex II and SAINT software packages<sup>63</sup> were used for data collection and data integration. Final cell constants were determined by global refinement of reflections from the complete data set. Data were corrected for systematic errors using SADABS.<sup>63</sup> Structure solutions and refinement were carried out using the SHELXTL-PLUS software package.<sup>64</sup> The structures were refined with full matrix least-squares refinement by minimizing Σw(F<sub>o</sub><sup>2</sup> - F<sub>c</sub><sup>2</sup>)<sup>2</sup>. All non-hydrogen atoms were refined anisotropically to convergence. All H atoms were added in the calculated position and were refined using appropriate riding models (AFIX m<sup>3</sup>). For 1, the benzothiazole ring atoms of one of the ligands were displaced over two positions which were refined with a site occupation factor of 0.5/0.5. Additional crystallographic details can be found in the Supporting Information.

**Acidity and Stability Constant Determination.** UV–vis pH titrations were employed for the determination of acidity constants of L1 and L2 and the stability constants of their Cu<sup>2+</sup> and Zn<sup>2+</sup> complexes. For acidity constants, solutions of BFCs (50 μM, 0.1 M NaCl, pH 3) were titrated with small aliquots of 0.1 M NaOH at room temperature. At least 30 UV–vis spectra were collected in the pH 3–11 range. Due to the limited solubility of L1 and L2 in water, MeOH stock solutions (10 mM) were used and titrations were performed in a MeOH–water mixture in which MeOH did not exceed 20% (v/v). Similarly, stability constants were determined by titrating solutions of L1 or L2 and equimolar amounts of Cu(ClO<sub>4</sub>)<sub>2</sub>·6H<sub>2</sub>O (50 μM or 0.5 mM) or Zn(ClO<sub>4</sub>)<sub>2</sub>·6H<sub>2</sub>O (50 μM) with small aliquots of 0.1 M NaOH at room temperature. At least 30 UV–vis spectra were collected in the pH 3–11 range. The acidity and stability constants were calculated using the HypSpec computer program (Protonic Software, U.K.).<sup>65</sup> Speciation plots of the compounds and their metal complexes were calculated using the program HySS2009 (Protonic Software, U.K.).<sup>66</sup>

**Amyloid β Peptide Experiments.** Aβ monomeric films were prepared by dissolving commercial Aβ<sub>42</sub> (or Aβ<sub>40</sub> for Aβ fibril binding studies) peptide (Keck Biotechnology Resource Laboratory, Yale University) in HFIP (1 mM) and incubating for 1 h at room temperature.<sup>67</sup> The solution was then aliquoted out and evaporated overnight. The aliquots were vacuum centrifuged and the resulting monomeric films stored at -80 °C. Aβ fibrils were generated by dissolving monomeric Aβ films in DMSO, diluting into the appropriate buffer, and incubating for 24 h at 37 °C with continuous agitation (final DMSO concentration was <2%). For metal-containing fibrils, the corresponding metal ions were added before the initiation of the fibrilization conditions. For inhibition studies, BFCs (50 μM, DMSO stock solutions) were added to Aβ solutions (25 mM) in the absence or presence of metal salts (CuCl<sub>2</sub> or ZnCl<sub>2</sub>, 25 μM) and incubated for 24 h at 37 °C with constant agitation. For disaggregation studies, the preformed Aβ fibrils in the absence or presence of metal ions were treated with BFCs and further incubated for 24 h at 37 °C with constant agitation. For preparation of soluble Aβ<sub>42</sub> oligomers a literature protocol was followed.<sup>14,67</sup> A monomeric film of Aβ<sub>42</sub> was dissolved in anhydrous DMSO, followed by addition of DMEM-F12 media (1:1 v/v, without phenol red, Invitrogen). The solution (50–100 μM) was incubated at 4 °C for 24 h and then centrifuged at 10000×g for 10 min. The supernatant was used as a solution of soluble Aβ<sub>42</sub> oligomers.

**Fluorescence Measurements.** All fluorescence measurements were performed using a SpectraMax M2e plate reader (Molecular Devices). For ThT fluorescence studies, samples were diluted to a final concentration of 2.5  $\mu\text{M}$   $A\beta$  in PBS containing 10  $\mu\text{M}$  ThT and the fluorescence measured at 485 nm ( $\lambda_{\text{ex}} = 435$  nm). For  $A\beta$  fibril binding studies, a 5  $\mu\text{M}$   $A\beta$  fibril solution was titrated with small amounts of compound and their fluorescence intensity measured ( $\lambda_{\text{ex}}/\lambda_{\text{em}} = 330/450$  nm). For ThT competition assays, a 5  $\mu\text{M}$   $A\beta$  fibril solution with 2  $\mu\text{M}$  ThT was titrated with small amounts of compound and the ThT fluorescence measured ( $\lambda_{\text{ex}}/\lambda_{\text{em}} = 435/485$  nm). For calculating  $K_i$  values, a  $K_d$  value of 1.17  $\mu\text{M}$  was used for the binding of ThT to  $A\beta$  fibrils (Figure S21b, Supporting Information).

**Fluorescence Microscopy.** A solution of  $A\beta_{42}$  fibrils in PBS (100  $\mu\text{M}$ ) was incubated with a 1 mg/mL EtOH solution of compound (final ratio of 4:1 v:v) for 10 min at room temperature. The fibrils were cleaned with distilled water and suspended in water–glycerol (2:1) before their analysis. Positive binding controls were performed under the same conditions with ThT. Images were obtained using with a Nikon A1Microscope (60 $\times$  lens) with 405 nm excitation and 450–500 nm emission range.

**Transmission Electron Microscopy (TEM).** Glow-discharged grids (Formar/Carbon 300-mesh, Electron Microscopy Sciences) were treated with  $A\beta$  samples (25  $\mu\text{M}$ , 5  $\mu\text{L}$ ) for 2–3 min at room temperature. Excess solution was removed using filter paper and grids were rinsed twice with  $\text{H}_2\text{O}$  (5  $\mu\text{L}$ ). Grids were stained with uranyl acetate (1% w/v,  $\text{H}_2\text{O}$ , 5  $\mu\text{L}$ ) for 1 min, blotted with filter paper, and dried for 15 min at room temperature. Images were captured using a FEI G2 Spirit Twin microscope (60–80 kV, 6500–97000 $\times$  magnification).

**Hydrogen Peroxide Assays.** Hydrogen peroxide production was determined using a HRP/Amplex Red assay.<sup>51,68–74</sup> A general protocol from Invitrogen's Amplex Red Hydrogen Peroxide/Peroxidase Assay kit was followed. Reagents were added directly to a 96-well plate in the following order to give a 100  $\mu\text{L}$  final solution:  $\text{CuCl}_2$  (100, 200, or 400 nM), phosphate buffer,  $A\beta$  peptide (200 nM), compounds (400 or 800 nM), sodium ascorbate (10  $\mu\text{M}$ ). The reaction was allowed to incubate for 30 min at room temperature. After this incubation, 50  $\mu\text{L}$  of freshly prepared working solution containing 100 nM Amplex Red (AnaSpec) and 0.2 U/mL HRP (Sigma) in phosphate buffer was added to each well, and the reaction was allowed to incubate for 30 min at room temperature. Fluorescence was measured using a SpectraMax M2e plate reader ( $\lambda_{\text{ex}}/\lambda_{\text{em}} = 530/590$ ). Error bars represent standard deviations for at least five measurements.

**Native Gel Electrophoresis and Western Blotting.** All gels, buffers, membranes, and other reagents were purchased from Invitrogen and used as directed except where otherwise noted. Samples were separated on 10–20% gradient Tris-tricine mini gels. The gel was transferred to a nitrocellulose membrane in an ice bath and the protocol was followed as suggested except that the membrane was blocked overnight at 4  $^\circ\text{C}$ . After blocking, the membrane was incubated in a solution (1:2000 dilution) of 6E10 anti- $A\beta$  primary antibody (Covance) for 3 h. Invitrogen's Western Breeze Chemiluminescent kit was used to visualize the bands. An alkaline-phosphatase antimouse secondary antibody was used, and the protein bands were imaged using a FUJIFILM Luminescent Image Analyzer LAS-1000CH.

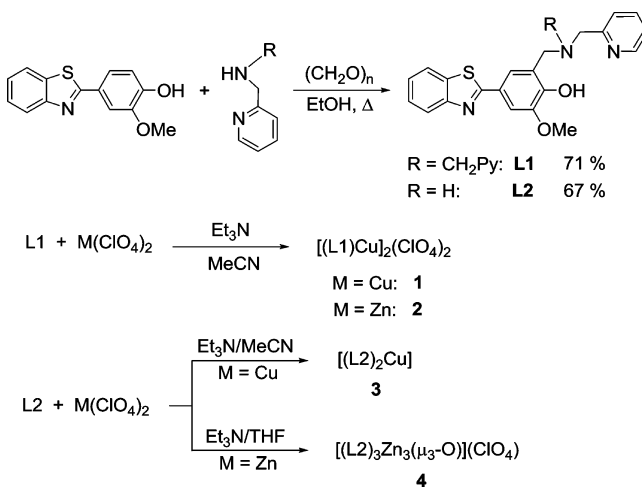
**Cytotoxicity Studies (Alamar Blue Assay).** Mouse neuroblastoma Neuro2A (N2A) cell lines were purchased from the American Type Culture Collection (ATCC). Cells were grown in DMEM/10% FBS, which is the regular growth media for N2A cells. N2A cells were plated to each well of a 96 well plate (2.5  $\times 10^4$ /well) with DMEM/10% FBS. The media was changed to DMEM/N2 media 24 h later. After 1 h, the reagents (20  $\mu\text{M}$   $A\beta_{42}$  species, compounds, and metals) were added. Due to the poor solubility of compounds in water or media, the final amount of DMSO used was 1% (v:v). After an additional incubation of 40 h, the Alamar blue solution was added in each well and the cells were incubated for 90 min at 37  $^\circ\text{C}$ . Absorbance was measured at 570 nm (control OD = 600 nm). For the toxicity studies, three types of  $A\beta_{42}$  species were tested: freshly made

monomeric  $A\beta_{42}$  ( $MA\beta_{42}$ ),  $A\beta_{42}$  oligomers ( $OA\beta_{42}$ ), and  $A\beta_{42}$  fibrils ( $FA\beta_{42}$ ). These  $A\beta_{42}$  species were prepared as described above.

## RESULTS AND DISCUSSION

**Synthesis and Characterization of L1 and L2.** Based on the linkage strategy for bifunctional chelator design (Scheme 1, approach A), we developed two compounds L1 and L2 that contain a 2-phenylbenzothiazole/vanillin group for  $A\beta$  binding<sup>59</sup> and a N-(2-pyridylmethyl) molecular fragment for metal chelation (Scheme 2).<sup>75,76</sup> The two BFCs were synthesized in good yields through the Mannich reaction of 2-(4-hydroxy-3-methoxy)benzothiazole<sup>62</sup> with paraformaldehyde and bis-(2-picolyl)amine for L1 or N-methyl-2-pyridinemethanamine for L2 (Scheme 3). The obtained compounds exhibit UV

Scheme 3. Synthesis of BFCs and their Metal Complexes



absorption bands in MeCN at 223 and 330 nm for L1 and 226 and 330 nm for L2 (Figures S8 and S9, Supporting Information). Due to the presence of the 2-phenylbenzothiazole group reminiscent of the amyloid-binding fluorescence dye thioflavin T (ThT), L1 and L2 exhibit fluorescence emission at  $\sim 450$  nm upon excitation at 330 nm, both in MeCN and PBS (Figures S14–S16, Supporting Information).

An important aspect of designing molecules for potential use in the central nervous system is their ability to cross the blood-brain barrier (BBB).<sup>31,77</sup> Considering the restrictive Lipinski's rules for BBB penetration ( $\text{MW} \leq 450$ ,  $\text{clogP} \leq 5$ , hydrogen bond donors  $\leq 5$ , hydrogen bond acceptors  $\leq 10$ , polar surface area  $\leq 90 \text{ \AA}^2$ ) and the calculated logBB values (Table S2, Supporting Information), both L1 and L2 satisfy these requirements, suggesting that these compounds should be capable of crossing the BBB.

**Acidity Constants of Compounds L1 and L2.** Since both L1 and L2 contain several acidic and basic functional groups, their acidity constants ( $\text{pK}_a$ ) were determined by UV–vis spectrophotometric titrations. For L1, UV–vis titrations from pH 3.0 to 11.0 reveal several changes in the spectra (Figure 1). The best fit to the data was obtained with four  $\text{pK}_a$  values: 4.875(5), 6.129(4), 8.462(2) and 10.356(1) (Table 1). Based on previously reported acidity constants for phenols, amines,<sup>78</sup> and pyridines,<sup>52</sup> we assigned the two lower  $\text{pK}_a$  values to the deprotonation of the two pyridinium groups, and the third  $\text{pK}_a$  value to the ammonium group. The highest  $\text{pK}_a$  value is likely due to phenol deprotonation in L1. For L2, UV–vis titrations from pH 3.0 to 11.0 reveal changes in the spectra (Figure 2)

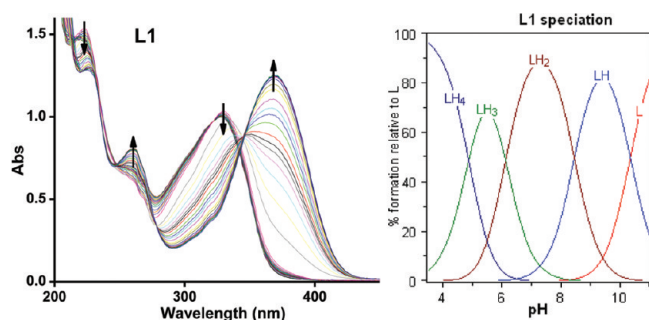


Figure 1. Variable pH (pH 3–11) UV spectra of L1 ( $[L1] = 50 \mu\text{M}$ ,  $25^\circ\text{C}$ ,  $I = 0.1 \text{ M NaCl}$ ) and species distribution plot.

Table 1. Acidity constants ( $\text{pK}_a$ 's) of L1 and L2 determined by spectrophotometric titrations (errors are for the last digit)

reaction	L1	L2
$[\text{H}_4\text{L}]^{3+} = [\text{H}_3\text{L}]^{2+} + \text{H}^+$ ( $\text{pK}_{a1}$ )	4.875(5)	1.94(1)
$[\text{H}_3\text{L}]^{2+} = [\text{H}_2\text{L}]^+ + \text{H}^+$ ( $\text{pK}_{a2}$ )	6.129(4)	6.393(4)
$[\text{H}_2\text{L}]^+ = [\text{HL}] + \text{H}^+$ ( $\text{pK}_{a3}$ )	8.462(2)	7.637(7)
$[\text{HL}] = [\text{L}]^- + \text{H}^+$ ( $\text{pK}_{a4}$ )	10.356(1)	10.037(4)

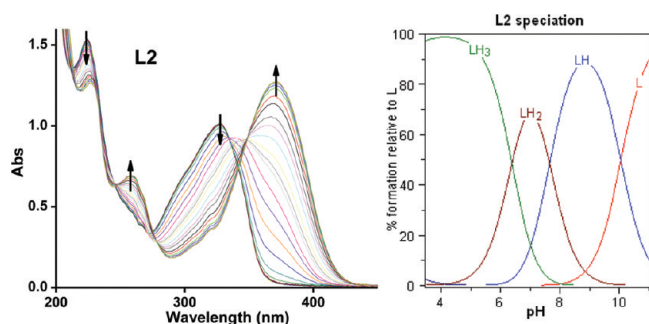


Figure 2. Variable pH (pH 3–11) UV spectra of L2 ( $[L2] = 50 \mu\text{M}$ ,  $25^\circ\text{C}$ ,  $I = 0.1 \text{ M NaCl}$ ) and species distribution plot.

that are also best fit with four  $\text{pK}_a$  values: 1.94(1), 6.393(4), 7.637(7) and 10.037(4) (Table 1). The highest three  $\text{pK}_a$  values can be assigned to the deprotonation of the pyridinium group, the ammonium group, and the phenol group, respectively, similar to the values obtained for L1. In addition, the low  $\text{pK}_a$  value of 1.94(1) is assigned to the deprotonation of the nitrogen atom of the benzothiazole group, similar to previous reports.<sup>79</sup>

#### Stability Constants for Metal Complexes of L1 and L2.

Similar spectrophotometric titrations were performed to determine the stability constants and solution speciation of  $\text{Cu}^{2+}$  and  $\text{Zn}^{2+}$  with L1 and L2. The  $\text{pK}_a$  values of the ligands and the deprotonation of metal-bound water molecules were included in the calculations.<sup>78</sup> The calculated values show that L1 exhibits larger binding constants ( $\log K$ 's) with  $\text{Cu}^{2+}$  and  $\text{Zn}^{2+}$  than the L2 ligand (Table 2) as expected given the additional metal-binding N-(2-pyridylmethyl) arm for L2. In addition, both L1 and L2 have a slightly higher affinity for  $\text{Cu}^{2+}$  than for  $\text{Zn}^{2+}$ . A visible spectrophotometric titration performed at a higher concentration of L1 and  $\text{Cu}^{2+}$  (0.5 mM) reveals spectral changes corresponding to the formation of the brown  $\text{Cu}(\text{L1})$  complex and confirms its high  $\log K$  value (Figure S1, Supporting Information).

Based on the obtained stability constants, solution speciation diagrams were calculated for  $\text{Cu}^{2+}$  and  $\text{Zn}^{2+}$  with L1 and L2

Table 2. Stability Constants ( $\log K$ 's) of the  $\text{Cu}^{2+}$  and  $\text{Zn}^{2+}$  Complexes of L1 and L2

reaction	$\log K$			
	L1		L2	
	$\text{Cu}^{2+}$	$\text{Zn}^{2+}$	$\text{Cu}^{2+}$	$\text{Zn}^{2+}$
$\text{M}^{2+} + \text{HL} = [\text{MHL}]^{+2}$	3.99(1)	6.68(5)	5.30(2)	6.12(3)
$\text{M}^{2+} + \text{L}^- = [\text{ML}]^+$	22.00(2)	16.52(1)	16.49(1)	15.19(1)
$[\text{ML}(\text{H}_2\text{O})]^{+1} = [\text{ML}(\text{OH})] + \text{H}^+$	-9.11(3)			

(Figures 3, 4, S2, and S3, Supporting Information). These diagrams suggest that in all four cases a 1:1 metal:ligand

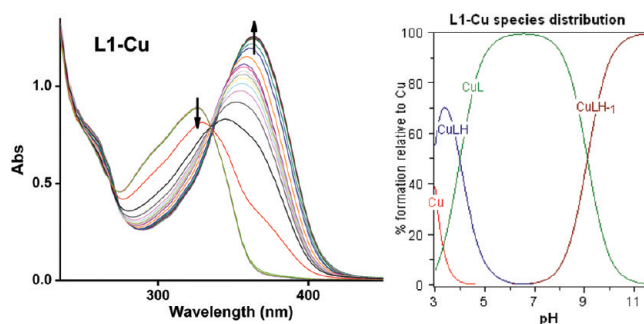


Figure 3. Variable pH (pH 3–11) UV spectra of L1 and  $\text{Cu}^{2+}$  system ( $[L1] = [\text{Cu}^{2+}] = 50 \mu\text{M}$ ,  $25^\circ\text{C}$ ,  $I = 0.1 \text{ M NaCl}$ ) and species distribution plot.

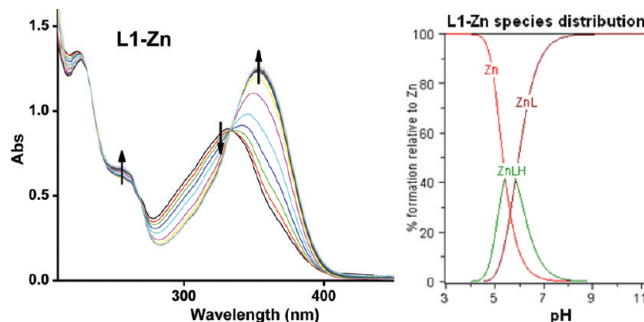


Figure 4. Variable pH (pH 3–11) UV spectra of L1 and  $\text{Zn}^{2+}$  ( $[L1] = [\text{Zn}^{2+}] = 50 \mu\text{M}$ ,  $25^\circ\text{C}$ ,  $I = 0.1 \text{ M NaCl}$ ) and species distribution plot.

complex is the predominant species formed (vide infra). In addition, Figures 3 and 4 show that the concentration of free  $\text{Cu}^{2+}$  with L1 is negligible above pH 4.5, while free  $\text{Zn}^{2+}$  is present up to pH 7.0. From the solution speciation diagrams the concentrations of unchelated  $\text{Cu}^{2+}$  and  $\text{Zn}^{2+}$  ( $\text{pM} = -\log[\text{M}_{\text{unchelated}}]$ ) at a specific pH value and total ion concentration can be calculated (Table 3). These pM values

Table 3. Calculated pM ( $-\log[\text{M}]_{\text{free}}$ ;  $\text{M} = \text{Zn}^{2+}$ ,  $\text{Cu}^{2+}$ ) for a Solution Containing a 1:1 Metal/Ligand Mixture ( $[\text{M}^{2+}]_{\text{tot}} = [\text{chelator}]_{\text{tot}} = 50 \mu\text{M}$ )

chelator	pZn		pCu
	pH 7.4	pH 6.6	pH 7.4
L1	8.0	9.6	10.4
L2	7.3	7.0	7.9
DTPA <sup>a</sup>	9.3	9.7	10.7

<sup>a</sup>Diethylenetriaminepentaacetic acid (DTPA), ref 80.

represent a direct estimate of the ligand–metal affinity by taking into account all relevant equilibria and thus can be used to compare the metal affinity among various ligands.<sup>78</sup> In our case, the pCu values for L1 are 9.6 and 10.4 at pH 6.6 and 7.4, respectively, while for L2 the values are 7.0 and 7.9, respectively. The pZn values at pH 7.4 were 8.0 and 7.3 for L1 and L2, respectively. Interestingly, these pM values are comparable to those calculated for the strong chelating agent DTPA (diethylenetriaminepentaacetic acid), suggesting that our compounds have a high metal-binding affinity, especially for Cu<sup>2+</sup> ions.<sup>80</sup>

Moreover, the calculated pCu and pZn for L1 and L2 can be used to predict the ability of these compounds to sequester metal ions from metal–A $\beta$  adducts. These pM values represent approximate dissociation constants and compare favorably with the  $K_d$  values reported for Cu–A $\beta$  (nM– $\mu$ M) and Zn–A $\beta$  ( $\mu$ M).<sup>26,29,31,57,78,81,82</sup> As such, the metal-binding affinities of L1 and L2 at relevant pH and metal ion concentrations strongly suggest their ability to chelate metal ions from metal–A $\beta$  species, supporting the observed role of these compounds in metal-mediated A $\beta$  aggregation (vide infra).

**Characterization of Metal Complexes.** The binding stoichiometry of L1 and L2 with Cu and Zn in solution was determined by Job's plot analysis.<sup>83</sup> For L1, a break at 0.5 mol fraction of metal ion suggests the formation of a 1:1 metal complex for both Cu<sup>2+</sup> and Zn<sup>2+</sup> ions (Figures S4 and S5, Supporting Information). For L2, formation of an 1:1 Cu<sup>2+</sup> complex in solution is suggested based on the break at 0.5 (Figure S6, Supporting Information), while for Zn<sup>2+</sup> the break between 0.33 and 0.5 indicates the formation of a mixture of 1:1 and 1:2 Zn:ligand complexes (Figure S7, Supporting Information). In addition, the presence of mononuclear Cu complexes in solution for both L1 and L2 was confirmed by the measured magnetic moments of  $\sim 1.73 \mu_B/\text{Cu}^{2+}$ .

The Cu and Zn complexes of L1 and L2 were synthesized following common procedures (Scheme 3) and their formation was confirmed by MS, <sup>1</sup>H NMR, and UV–vis spectroscopy. Cu complexes **1** and **3** show characteristic *d–d* transition bands (i.e., 832 nm for **1** and 660 nm for **3**) as well as phenolate-to-Cu charge transfer bands (425 nm for **1** and 520 nm for **3**, Figures S10 and S12, Supporting Information). For Zn<sup>2+</sup> complexes **2** and **4**, the ligand-based absorption bands at  $\sim 330$  nm shift to  $\sim 350$  nm upon complex formation (Figures S11 and S13, Supporting Information). As expected, the observed ligand fluorescence is quenched by the Cu<sup>2+</sup> ion in **1** and **3**. However, the presence of Zn<sup>2+</sup> causes a significant enhancement of the emission intensity in **2** and **4**, (Figures S17 and S18, Supporting Information), similar to the reported Zn fluorescent sensors containing N-(2-pyridylmethyl) arms.<sup>75,76</sup>

**X–ray Structure of Metal Complexes.** Complexes **1–4** were characterized by X–ray crystallography, and the relevant bond distances and bond angles are given in Tables S3–S6 (Supporting Information). The structures of the complexes **1** and **2** of L1 with Cu and Zn, respectively, reveal the formation in the solid state of dinuclear complexes with a 2:2 metal:ligand stoichiometry (Scheme 3). Each metal ion is bound to the two pyridine N's and the amine N atom of one ligand molecule, while the two phenolate O's bridge the two metal centers (Figures 5a and S19, Supporting Information). Both Cu<sup>2+</sup> centers in **1** exhibit a distorted square–pyramidal coordination geometry with trigonality index parameters<sup>84</sup>  $\tau$  of 0.32 and 0.44, respectively. By comparison, the  $\tau$  values of 0.63 and 0.50 support a distorted trigonal bipyramidal geometry for the Zn<sup>2+</sup>

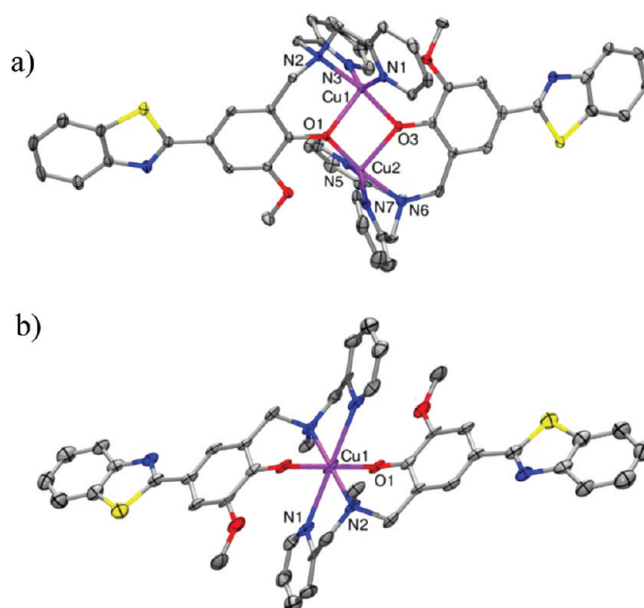


**Figure 5.** ORTEP view of (a) the dication of **1** and (b) **3** with 50% probability ellipsoids. All hydrogen atoms, counteranions, and solvent molecules are omitted for clarity. Selected bond distances, **1**: Cu(1)–Cu(2) 3.0848(2), Cu1–N1 2.0024(19), Cu1–N2 2.0179(18), Cu1–N3 2.022(2), Cu1–O1 2.1260(16), Cu1–O3 1.9357(16), Cu2–N5 1.985(2), Cu2–N6 2.0281(19), Cu2–N7 1.992(2), Cu2–O3 2.1479(16); **3**: Cu–N1 2.563(5), Cu–N2 2.102(4), Cu–O1 1.956(4).

centers in **2**. Interestingly, while L2 forms a 2:1 complex with Cu<sup>2+</sup> in which the metal center adopts a pseudo–octahedral coordination environment (Figure 5b), reactions of L2 with Zn<sup>2+</sup> leads to formation of a symmetric trinuclear complex **4** in which each Zn center exhibits a distorted square pyramidal geometry with a  $\tau$  value of 0.29 (Figure S20, Supporting Information). Similar to **2**, the Zn<sup>2+</sup> ions in **4** are bridged by the phenolate O's of the L2 ligand, and an additional  $\mu_3$ -oxo group bridges all three Zn centers.

While L1 is a tetradentate ligand and thus is expected to form 1:1 Cu and Zn complexes, L2 is a tridentate ligand that can generate metal complexes with different stoichiometry in solution versus the solid state. Notably, while the solid state structure for **3** shows a 1:2 Cu:ligand complex, the Job's plot analysis and UV–vis titrations suggest the formation of a 1:1 complex in solution. In addition, the Zn–L2 complex **4** is isolated as a 1:1 complex in the solid state, yet the Job's plot analysis suggests formation of a mixture of 1:1 and 1:2 complexes in solution.

**Interaction of L1 and L2 with A $\beta$  Species.** The compounds described herein contain a 2-phenylbenzothiazole fragment reminiscent of Thioflavin T (ThT), a common fluorescent dye used to detect the  $\beta$  sheet structure of fibrillar A $\beta$  aggregates. In this context, the affinity of L1 and L2 toward A $\beta$  fibrils was investigated by fluorescence spectroscopy. These studies were performed with A $\beta$  fibrils obtained from the A $\beta_{40}$  peptide, which forms more homogeneous fibrillar structures without any nonfibrillar aggregates (Figure S21a, Supporting Information).<sup>85,86</sup> Interestingly, an increase in the emission intensity of L1 is observed in presence of A $\beta$  fibrils (Figure S22a, Supporting Information). When a solution of A $\beta$  fibrils was titrated with L1 and the emission intensity increase corrected for the intrinsic fluorescence of L1, a saturation

behavior is observed that is best fit with a one-site binding model to give a  $K_d$  of  $135 \pm 25$  nM (Figure 6a). This value

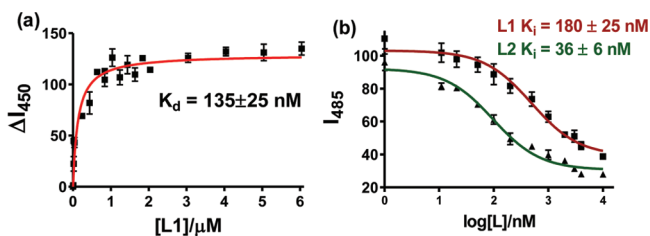


**Figure 6.** (a) Fluorescence titration assay of L1 with  $A\beta$  fibrils ( $[A\beta] = 5 \mu\text{M}$ ,  $\lambda_{\text{ex}}/\lambda_{\text{em}} = 330/450$  nm); (b) ThT fluorescence competition assays with L1 and L2 ( $[A\beta] = 5 \mu\text{M}$ ,  $[\text{ThT}] = 2 \mu\text{M}$ ).

suggests that L1 exhibits a high affinity for the  $A\beta$  fibrils comparable to other neutral ThT derivatives,<sup>85,87</sup> suggesting that appending a metal-binding group to the 2-phenylbenzothiazole fragment does not limit its amyloid binding affinity. By comparison, performing the same titration of  $A\beta$  fibrils with ThT yields a  $K_d$  of  $1.17 \pm 0.14 \mu\text{M}$  (Figure S21b, Supporting Information), a value similar to those reported previously.<sup>85,87</sup>

The L2 compound exhibits an increased fluorescence intensity compared to L1, yet its emission does not change in presence of  $A\beta$  fibrils (Figure S22b, Supporting Information). This behavior is likely not due to the lack of L2 binding to  $A\beta$  fibrils, but is merely a failure of  $A\beta$  to impact the fluorescence of L2.<sup>88</sup> Indeed, a ThT fluorescence competition assay performed by addition of L1 or L2 to a solution of  $A\beta$  fibrils in presence of ThT shows a dramatic decrease in ThT fluorescence upon addition of nanomolar amounts of BFCs. A control experiment performed in absence of  $A\beta$  fibrils confirms that L1 and L2 do not quench the ThT fluorescence. Titrations with various amounts of compounds reveal competitive binding curves that yield  $K_i$  values  $180 \pm 25$  nM and  $36 \pm 6$  nM for L1 and L2, respectively (Figure 6b).<sup>86,87</sup> While the  $K_i$  value for L1 is similar to the  $K_d$  value obtained directly, the  $K_i$  value obtained for L2 shows an even stronger binding affinity to  $A\beta$  fibrils. Overall, these studies strongly suggest that the tested BFCs bind tightly to  $A\beta$  fibrils and that appending a metal-binding arm to the 2-phenylbenzothiazole group does not negatively affect the amyloid binding affinity of these compounds. While other reported BFCs have employed benzothiazole fragments as amyloid-binding motifs, no binding affinities for the  $A\beta$  species have been measured for those systems.<sup>49,53,54</sup> Moreover, L1 and L2 represent to the best of our knowledge the first bifunctional metal-chelators for which the  $A\beta$  fibril binding affinities were measured directly.<sup>89</sup>

To test the bifunctional character of the synthesized compounds, the  $A\beta$  fibrils were treated with  $\text{Zn}^{2+}$  ions and employed in a ThT competition assay, in order to test the amyloid-binding ability of L1 and L2 in presence of metal ions. The ThT competition binding assays with the  $\text{Zn}-A\beta$  fibrils yield  $K_i$  value of  $275 \pm 40$  nM and  $270 \pm 40$  nM for L1 and L2, respectively (Figure S23, Supporting Information). While the  $K_i$  value for L1 in presence of  $\text{Zn}^{2+}$  is less than 2-fold larger than that in absence of  $\text{Zn}^{2+}$ , a 7-fold difference is observed for L2. This suggests that the amyloid binding affinity is more sensitive to the presence of metal ions for the latter compound, possibly due to its weaker metal-binding ability and the formation of a 1:2 metal complex in solution (vide supra). Similar amyloid-

binding competition assays could not be performed in presence of  $\text{Cu}^{2+}$  due to quenching of ThT fluorescence.

**Fluorescence Microscopy Binding Assays.** The emission properties of L1 and L2 were further explored by fluorescence microscopy studies of  $A\beta$  fibrils, a complementary method for assessing the interaction of such compounds with amyloid fibrils.<sup>57</sup> Incubation of ThT, L1, and L2 with  $A\beta_{42}$  fibrils for 10 min followed by fluorescence microscopy imaging shows that the areas rich in  $A\beta_{42}$  aggregates exhibit a bright blue fluorescence, the emission intensity for L1 and L2 being similar to that observed for ThT (Figure 7). These studies provide

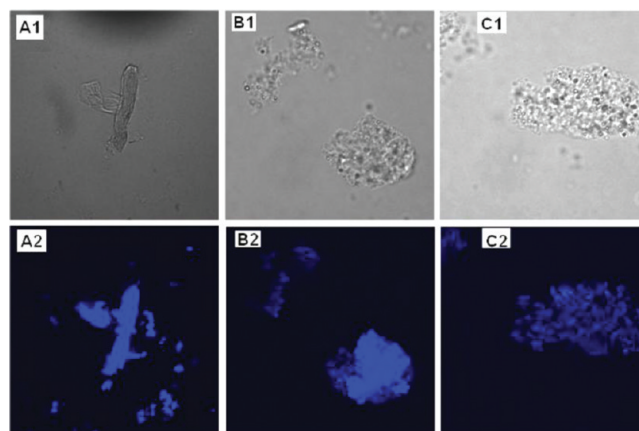


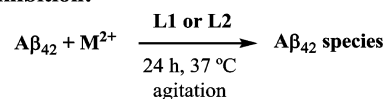
**Figure 7.** Visualization of  $A\beta_{42}$  fibrils stained with (A) ThT, (B) L1, and (C) L2. Panels A1–C1, phase-contrast microscopy images to account for the presence of fibrils; panels A2–C2, fluorescence microscopy images (magnification =  $60\times$ ,  $\lambda_{\text{ex}} = 405$  nm).

further evidence that the tested BFCs exhibit both amyloid-binding affinity and fluorescence properties similar to ThT and thus constitute molecular motifs that can be used in future studies for the development of novel amyloid-binding compounds.

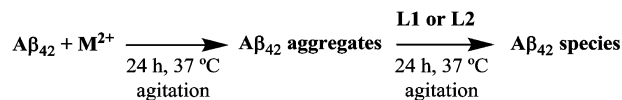
**Effect of L1 and L2 on  $A\beta_{42}$  Aggregation.** Having confirmed the bifunctionality of L1 and L2 through metal-chelating and  $A\beta$ -binding studies, we explored the ability of these molecules to modulate the metal-mediated aggregation of the  $A\beta_{42}$  peptide (Scheme 4). To the best of our knowledge, our

#### Scheme 4. Inhibition and Disaggregation Experiments

##### Inhibition:



##### Disaggregation:



$A\beta$  aggregation studies with bifunctional chelators are the first to use the more aggregation-prone  $A\beta_{42}$  peptide, which was also shown to form neurotoxic soluble  $A\beta$  oligomers.<sup>18–20</sup> For these experiments, freshly prepared monomeric  $A\beta_{42}$  solutions were treated with metal ions, BFCs, or both. In these studies, the measurement of ThT fluorescence intensity is not a viable method to quantify the extent of  $A\beta$  aggregation, since L1 and

L2 dramatically reduce the ThT emission intensity due to their competitive binding to  $A\beta$  fibrils (Figure S24, Supporting Information). In addition, both  $Cu^{2+}$  and  $Zn^{2+}$  ions lead to a reduced ThT fluorescence, due to emission quenching by the paramagnetic  $Cu^{2+}$  ions or  $Zn^{2+}$ -induced formation of non-fibrillar  $A\beta$  aggregates.<sup>41,90</sup> A more quantitative analysis of the  $A\beta$  aggregation studies is provided by native gel electrophoresis/Western blot analysis and transmission electron microscopy (TEM) techniques. While the former type of analysis reveals the presence of smaller, soluble  $A\beta$  aggregates and their molecular weight distribution, the latter method allows the characterization of the larger, insoluble  $A\beta$  aggregates that cannot be analyzed by gel electrophoresis. Thus, the use of both these methods provides a more complete picture of the extent and pathways of  $A\beta$  aggregation under various conditions.<sup>51,52</sup>

The aggregation of  $A\beta_{42}$  for 24 h at 37 °C leads to well-defined  $A\beta$  fibrils, as confirmed by TEM (Figure 8a), and native

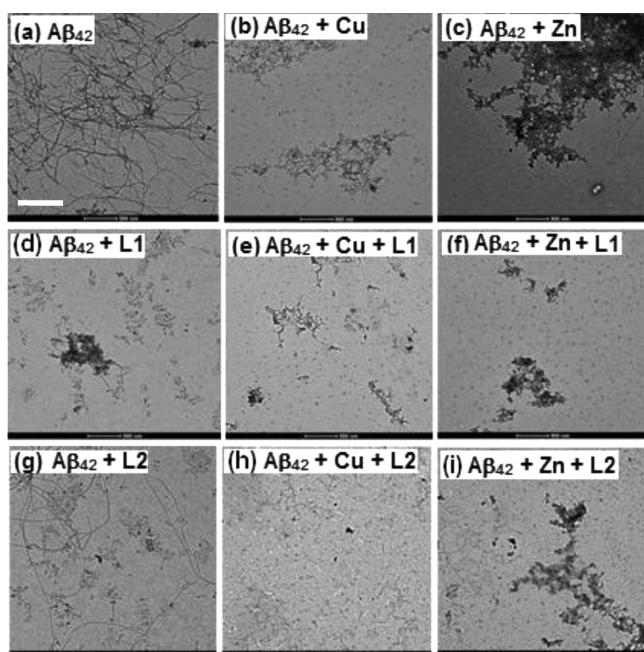


**Figure 8.** TEM images of the inhibition of  $A\beta_{42}$  aggregation by L1 and L2, in the presence or absence of metal ions ( $[A\beta_{42}] = [M^{2+}] = 25 \mu M$ ,  $[compound] = 50 \mu M$ , 37 °C, 24 h, scale bar = 500 nm). Samples: (a)  $A\beta_{42}$ ; (b)  $A\beta_{42} + Cu^{2+}$ ; (c)  $A\beta_{42} + Zn^{2+}$ ; (d)  $A\beta_{42} + L1$ ; (e)  $A\beta_{42} + L1 + Cu^{2+}$ ; (f)  $A\beta_{42} + L1 + Zn^{2+}$ ; (g)  $A\beta_{42} + L2$ ; (h)  $A\beta_{42} + L2 + Cu^{2+}$ ; (i)  $A\beta_{42} + L2 + Zn^{2+}$ .

gel/Western blot analysis shows a small amount of soluble  $A\beta$  oligomers (Figure 9a). However,  $A\beta$  aggregation in presence of Cu shows formation of almost no  $A\beta$  fibrils by TEM (Figure 8b), while Western blotting shows the formation of soluble  $A\beta_{42}$  oligomers with masses in the 10–110 kDa range (Figure 9b). By comparison, the aggregation of  $A\beta_{42}$  in presence of  $Zn^{2+}$  leads to a small amount of amorphous aggregates (Figure 8c), and native gel/Western blot analysis shows formation of soluble  $A\beta_{42}$  oligomers of various sizes (Figure 9c).<sup>90</sup> These results suggest that metal ions are able to stabilize the soluble  $A\beta_{42}$  oligomers and thus partially inhibit the  $A\beta_{42}$  aggregation.<sup>91</sup> This is in contrast with a large number of reports showing the aggregation-promoting effect of metal ions on the  $A\beta$  peptide.<sup>23–27,29–32,37,38</sup> However, most of these previous

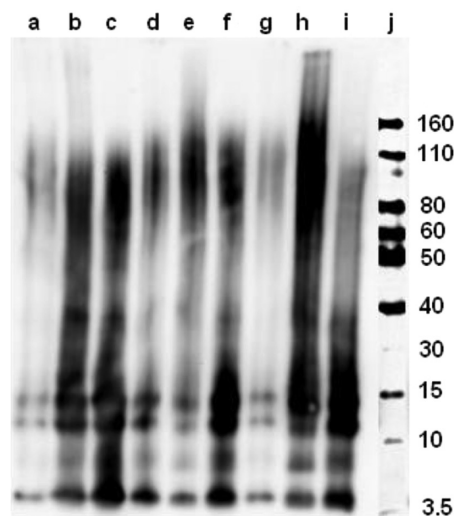


**Figure 9.** Native gel electrophoresis/Western blot analysis for the inhibition of  $A\beta_{42}$  aggregation by L1 and L2, in the presence or absence of metal ions ( $[A\beta_{42}] = [M^{2+}] = 25 \mu M$ ,  $[compound] = 50 \mu M$ , 37 °C, 24 h). Lanes are as follows: (a)  $A\beta_{42}$ ; (b)  $A\beta_{42} + Cu^{2+}$ ; (c)  $A\beta_{42} + Zn^{2+}$ ; (d)  $A\beta_{42} + L1$ ; (e)  $A\beta_{42} + L1 + Cu^{2+}$ ; (f)  $A\beta_{42} + L1 + Zn^{2+}$ ; (g)  $A\beta_{42} + L2$ ; (h)  $A\beta_{42} + L2 + Cu^{2+}$ ; (i)  $A\beta_{42} + L2 + Zn^{2+}$ ; and (j) MW marker.

studies have employed the  $A\beta_{40}$  peptide that follows a more direct aggregation pathway to form homogeneous, well-defined fibrillar structures.<sup>85,86</sup> Detailed metal-mediated aggregation studies of monomeric  $A\beta_{42}$  are currently underway in order to decipher the complex aggregation pathways that include soluble  $A\beta_{42}$  oligomers and nonfibrillar aggregates.<sup>92,93</sup>

Interestingly, both L1 and L2 were observed to be good inhibitors of aggregation, noticeably fewer  $A\beta_{42}$  fibrils being observed in presence vs the absence of these compounds (Figure 8d and g). When  $A\beta$  aggregation is performed in presence of both compounds and metal ions, TEM analysis shows no  $A\beta$  fibril formation. While  $Cu^{2+}$  and L1 or L2 leads to complete disappearance of any large aggregates (Figure 8e and h), the presence of  $Zn^{2+}$  and L1 or L2 generates only a small amount of amorphous nonfibrillar aggregates (Figure 8f and i). Native gel/Western blot analysis shows formation of a wide range of soluble  $A\beta_{42}$  oligomers, including higher-mass aggregates, in the presence of Cu and L1 or L2 (Figure 9e and h), L2 having a more pronounced effect. Presence of  $Zn^{2+}$  and L1 or L2 leads to a higher amount of small  $A\beta_{42}$  oligomers with masses of 10–30 kDa (Figure 9f and i). These studies clearly show the metal ions and compounds tested have an inhibitory effect on  $A\beta_{42}$  fibrillization, suggesting that these bifunctional chelators can modulate the neurotoxicity of the formed  $A\beta_{42}$  species (vide infra).

**Disaggregation of  $A\beta$  Aggregates by L1 and L2.** The ability of L1 and L2 to disaggregate preformed  $A\beta_{42}$  fibrils was also studied (Scheme 4). The  $A\beta_{42}$  fibrils (formed by incubating for 24 h at 37 °C) were incubated with BFCs for an additional 24 h at 37 °C and analyzed by TEM and native gel/Western blotting (Figure 10). The 48 h total incubation leads to mature  $A\beta_{42}$  fibrils, as observed by TEM (Figure 10, panel a) while the Western blot shows the presence of higher order  $A\beta_{42}$  oligomers (Figure 10, lane a), likely due to an assembly disassembly equilibrium that is established for mature  $A\beta$  fibrils.<sup>91–93</sup> While the presence of  $Cu^{2+}$  or  $Zn^{2+}$  during the initial 24 h incubation at 37 °C leads to formation of smaller

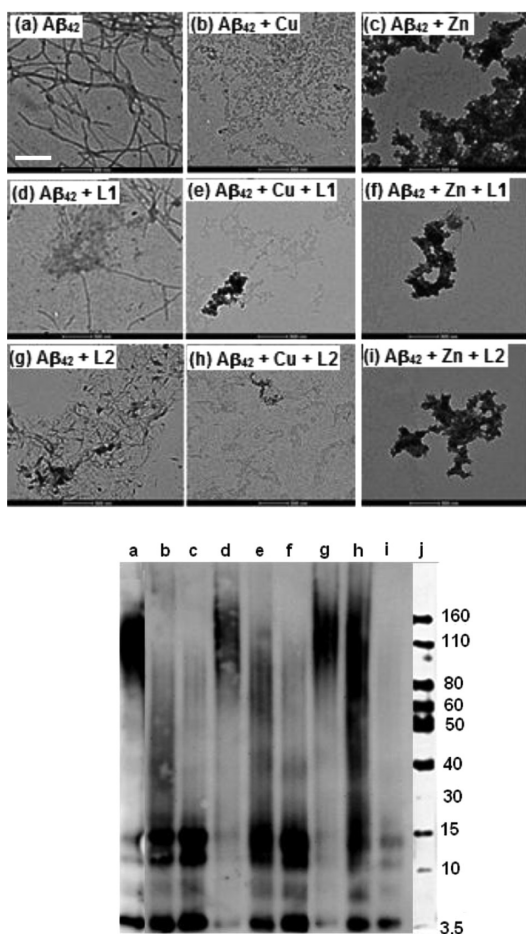


**Figure 10.** (Top) TEM images of  $A\beta$  species from disaggregation experiments ( $[A\beta] = [M^{2+}] = 25 \mu\text{M}$ ,  $[\text{compound}] = 50 \mu\text{M}$ ,  $37^\circ\text{C}$ , 24 h, scale bar = 500 nm). (Bottom) Native gel electrophoresis/Western blot analysis. Panels and lanes are as follows: (a)  $A\beta$ ; (b)  $A\beta + \text{Cu}^{2+}$ ; (c)  $A\beta + \text{Zn}^{2+}$ ; (d)  $A\beta + \text{L1}$ ; (e)  $A\beta + \text{L1} + \text{Cu}^{2+}$ ; (f)  $A\beta + \text{L1} + \text{Zn}^{2+}$ ; (g)  $A\beta + \text{L2}$ ; (h)  $A\beta + \text{L2} + \text{Cu}^{2+}$ ; (i)  $A\beta + \text{L2} + \text{Zn}^{2+}$ ; and (j) MW marker.

aggregates and soluble oligomers (Figure 8b and c; Figure 9b and c), the additional 24 h incubation leads to mature  $A\beta$  aggregates (Figure 10, panels b and c) along with a decrease in the amount of soluble  $A\beta$  oligomers (Figure 10, lanes b and c). Addition of L1 or L2 to  $A\beta_{42}$  fibrils leads to a dissociation of the large  $A\beta_{42}$  aggregates, as observed by TEM (Figure 10, panels d and g), although small  $A\beta_{42}$  fibrils are still present. By contrast, the disaggregation effect of L1 and L2 is more pronounced in presence of  $\text{Cu}^{2+}$  or  $\text{Zn}^{2+}$ . The  $\text{Cu}^{2+}$ - $A\beta_{42}$  aggregates are efficiently disassembled by L1 and especially by L2 to form a wide range of soluble  $A\beta_{42}$  oligomers of various sizes (Figure 10, lanes e and h), which are expected to lead to increased neurotoxicity (vide infra). This effect is similar to that observed for the inhibition of  $A\beta_{42}$  aggregation by L1 and L2 in presence of  $\text{Cu}^{2+}$  (Figure 9e and h). The addition of L1 and L2 to  $\text{Zn}^{2+}$ - $A\beta_{42}$  aggregates generates a small amount of amorphous nonfibrillar aggregates (Figure 10, panels f and j). Overall, both inhibition and disaggregation studies show that L1 and L2 are able to control the  $A\beta$  aggregation process both in the absence and presence of metal ions, highlighting the bifunctional character of these compounds.

**Control of  $\text{Cu}$ - $A\beta$   $\text{H}_2\text{O}_2$  Production by L1 and L2.** The interaction of the  $A\beta$  peptides with redox-active metal ions such

as  $\text{Cu}^{2+}$  has been proposed to lead to formation of ROS (e.g.,  $\text{H}_2\text{O}_2$ ) and oxidative stress associated with  $A\beta$  neurotoxicity.<sup>3,26–31,33–36</sup> As such, the developed BFCs should ideally be able to control ROS formation.<sup>30,36,51</sup> The effect of L1 and L2 on  $\text{H}_2\text{O}_2$  production by  $\text{Cu}^{2+}$ - $A\beta_{42}$  species was examined using the HRP/Amplex Red assay.<sup>35,51,68,74</sup> Under reducing conditions, the  $\text{Cu}^{2+}$ - $A\beta_{42}$  species react with  $\text{O}_2$  to generate  $\text{H}_2\text{O}_2$  (Figure S25, Supporting Information). Addition of L1 to such a solution reduces the production of  $\text{H}_2\text{O}_2$  by >65% for the  $\text{Cu}$ - $A\beta_{42}$  species. L2 shows an even more pronounced effect, almost completely eliminating (>90%)  $\text{H}_2\text{O}_2$  production (Figure S25, Supporting Information). By comparison, other metal chelators such as clioquinol (CQ) and phenanthroline (phen) have almost no effect on  $\text{H}_2\text{O}_2$  production, while the strong chelator ethylenediaminetetraacetic acid (EDTA) shows a reduction in  $\text{H}_2\text{O}_2$  formation similar to that of L2. Interestingly, the metal-binding compound *N*-methyl-*N,N*-bis(2-pyridylmethyl)amine (L\*), which resembles the metal-chelating fragments in L1 and L2, exhibits also a dramatic reduction of  $\text{H}_2\text{O}_2$  production by  $\text{Cu}^{2+}$  and  $\text{Cu}^{2+}$ - $A\beta_{42}$  species (Figure S25, Supporting Information), suggesting an intrinsic antioxidant property of this metal-binding molecular fragment. Overall, these results support not only the strong chelating ability of L1 and L2 for  $\text{Cu}^{2+}$ , but also their ability to control ROS formation and the redox properties of both free  $\text{Cu}^{2+}$  and  $\text{Cu}^{2+}$ - $A\beta_{42}$  species, important multifunctional features needed for the future use of these compounds *in vivo*.

**Effect of L1 and L2 on  $A\beta_{42}$  Neurotoxicity in Neuronal Cells.** Since metal- $A\beta$  species have been shown to be neurotoxic,<sup>25,51,94</sup> development of compounds that will control this toxicity is desired. In this context, we investigated the effect of L1 and L2 on metal- $A\beta$  neurotoxicity in Neuro-2A (N2A)<sup>92</sup> cells using an Alamar Blue cell viability assay, which has been shown to give more reproducible results than the MTT assay.<sup>95,96</sup> First, we observe a limited neurotoxicity of  $A\beta_{42}$  fibrils ( $86 \pm 8\%$  cell viability, Figure 11, lane 1), while the presence of both  $A\beta_{42}$  fibrils and  $\text{Cu}^{2+}$  shows no cell death (Figure 11, lane 3), supporting the previously reported diminished toxicity of  $A\beta_{42}$  fibrils.<sup>14–17,19</sup> Second, we tested

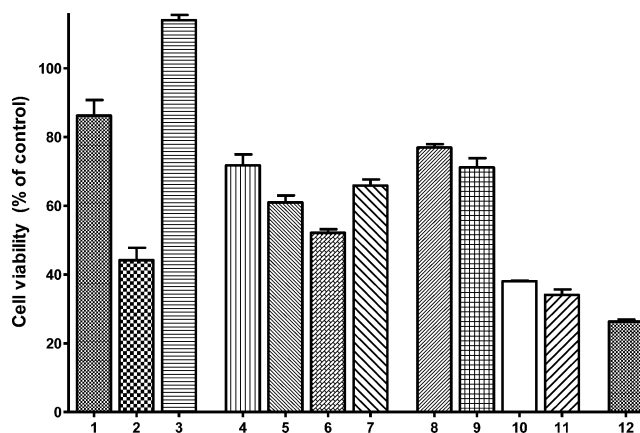


**Figure 11.** Cell viability (% control) upon incubation of Neuro2A cells with (1)  $A\beta_{42}$  fibrils ( $FA\beta_{42}$ ); (2)  $A\beta_{42}$  oligomers ( $OA\beta_{42}$ ); (3)  $FA\beta_{42} + \text{Cu}^{2+}$ ; (4) L1; (5) L1 +  $\text{Cu}^{2+}$ ; (6)  $MA\beta_{42} + \text{L1} + \text{Cu}^{2+}$ ; (7)  $FA\beta_{42} + \text{L1} + \text{Cu}^{2+}$ ; (8) L2; (9) L2 +  $\text{Cu}^{2+}$ ; (10)  $MA\beta_{42} + \text{L2} + \text{Cu}^{2+}$ ; (11)  $FA\beta_{42} + \text{L2} + \text{Cu}^{2+}$ ; and (12)  $FA\beta_{42} + \text{CQ} + \text{Cu}^{2+}$ . Conditions:  $[\text{Compound}] = 2 \mu\text{M}$ ;  $[\text{Cu}^{2+}] = 20 \mu\text{M}$ ;  $[A\beta_{42}] = 20 \mu\text{M}$ .

the neurotoxicity of our compounds, which shows that L1 and L2 exhibit  $72 \pm 4\%$  and  $77 \pm 2\%$  cell survival, respectively, when used in  $2 \mu\text{M}$  concentrations (Figure 11, lanes 4 and 8). By comparison, the clinically tested compound CQ shows  $<30\%$  cell survival at concentrations  $>2 \mu\text{M}$ , while EDTA shows  $90\text{--}95\%$  cell survival up to  $20 \mu\text{M}$  concentration (Figure S26, Supporting Information).<sup>51,52</sup> While our compounds show a more pronounced toxicity at  $20 \mu\text{M}$ , their effect on the metal- $A\beta$  species toxicity can be evaluated at  $2 \mu\text{M}$  given their high affinity for both metal ions and  $A\beta$  species.<sup>97</sup> The toxicity of L1 and L2 was tested also in presence of  $\text{Cu}^{2+}$  to show only a slight decrease in cell viability (Figure 11, lanes 5 and 9).

The effect of L1 and L2 on  $A\beta_{42}$ -induced neurotoxicity was investigated under both inhibition conditions (i.e., in presence of monomeric  $A\beta_{42}$ ) and disaggregation conditions (i.e., in presence of preformed  $A\beta_{42}$  fibrils). The presence of monomeric  $A\beta_{42}$  ( $20 \mu\text{M}$ ), L1 ( $2 \mu\text{M}$ ), and  $\text{Cu}^{2+}$  ( $20 \mu\text{M}$ ) leads to  $52 \pm 3\%$  cell viability, while a  $65 \pm 5\%$  cell survival was observed in presence of  $A\beta_{42}$  fibrils (Figure 11, lanes 6 and 7, respectively). Interestingly, treatment of the N2A cells with  $A\beta_{42}$  ( $20 \mu\text{M}$ ), L2 ( $2 \mu\text{M}$ ), and  $\text{Cu}^{2+}$  ( $20 \mu\text{M}$ ) dramatically lowers the cell survival to  $38 \pm 2\%$  under inhibition conditions (Figure 11, lane 10) and  $34 \pm 4\%$  under disaggregation conditions (Figure 11, lane 11). This increased neurotoxicity of  $A\beta_{42}$  species in presence of  $\text{Cu}^{2+}$  and L2 is most likely due to the formation of a range of soluble  $A\beta_{42}$  oligomers of various sizes, as observed by Western blotting in the inhibition and disaggregation studies (lanes h in Figures 9 and 10). This is confirmed by the decreased cell survival of  $44 \pm 8\%$  in presence of soluble  $A\beta_{42}$  oligomers (Figure 11, lane 2), supporting the increased neurotoxicity of  $A\beta_{42}$  oligomers versus  $A\beta_{42}$  fibrils.<sup>16,19</sup> The formation of larger soluble  $A\beta_{42}$  oligomers in presence of L1 is not as pronounced as that observed for L2 (Figures 9 and 10, lanes h vs e), which likely leads to an increased cell survival for L1 vs L2 (Figure 11, lanes 10–11 vs 6–7). As expected, addition of CQ to  $A\beta_{42}$  fibrils in presence of  $\text{Cu}^{2+}$  leads to marked cell toxicity (Figure 11, lane 12), likely due to the ability of CQ to disaggregate  $A\beta$  fibrils.<sup>98</sup>

These cell toxicity results provide another perspective on the neurotoxicity of metal- $A\beta$  species. Almost all previous studies investigating the effect of bifunctional compounds on the neurotoxicity of metal- $A\beta$  species have focused on the less neurotoxic and possibly even anti-amyloidogenic  $A\beta_{40}$  peptide.<sup>9,99,100</sup> Except for one recent report,<sup>101</sup> compounds that inhibit metal-mediated  $A\beta_{40}$  aggregation or promote disaggregation of amyloid fibrils were shown to lead to increased cell viability.<sup>49,51,52</sup> However, this approach may not be optimal for the  $A\beta_{42}$  peptide, given the increased toxicity observed for the soluble  $A\beta_{42}$  oligomers.<sup>92</sup> Future studies aimed at the development of bifunctional chelators that control the metal- $A\beta$  neurotoxicity *in vivo* should take into consideration the formation of neurotoxic soluble  $A\beta_{42}$  oligomers and their proposed role in AD neuropathogenesis.

## SUMMARY

The use of chemical agents that can modulate the interaction of metal ions with the  $A\beta$  peptide can be a useful tool in studying the role of metal ions and metal- $A\beta$  species in AD neuropathogenesis. In this regard, we employed a linking strategy to design a new family of bifunctional chelators that bind metal ions and can also interact with  $A\beta$  species. The bifunctional character of the synthesized compounds L1 and L2 was confirmed by metal-chelating and  $A\beta$ -binding studies. First,

both compounds were found to bind  $\text{Cu}^{2+}$  and  $\text{Zn}^{2+}$  with high affinities, and their corresponding complexes were synthesized and structurally characterized. Second, L1 and L2 exhibit high affinity toward  $A\beta$  species, as determined through fluorescence titration assays and fluorescence microscopy studies. These BFCs were able to inhibit the metal-mediated  $A\beta$  aggregation and disassemble preformed  $A\beta$  fibrils, as well as dramatically reduce  $\text{H}_2\text{O}_2$  formation by  $\text{Cu}^{2+}$ - $A\beta$  species, thus exhibiting also an antioxidant functionality. Most notably, this is the first detailed study of the interaction of bifunctional compounds with the more aggregation-prone  $A\beta_{42}$  peptide, which forms neurotoxic soluble  $A\beta_{42}$  oligomers. Intriguingly, the ability of the developed BFCs to inhibit  $A\beta$  fibril formation and promote fibril disaggregation leads to increased cellular toxicity, especially for L2, which is likely due to formation of soluble  $A\beta_{42}$  oligomers of various sizes. These studies suggest that the previously employed strategy of inhibiting  $A\beta_{40}$  aggregation and amyloid fibril disaggregation may not be optimal for the  $A\beta_{42}$  peptide, due to formation of neurotoxic soluble  $A\beta_{42}$  oligomers. Future bifunctional chelator design strategies should be aimed at controlling these soluble  $A\beta_{42}$  oligomers, especially for *in vivo* studies and potential AD therapeutics development.

## ASSOCIATED CONTENT

### Supporting Information

X-ray crystallographic files in CIF format, crystallographic data for 1–4, spectrophotometric titrations, Job's plots, UV–vis and fluorescence spectra for L1, L2 and metal complexes, ORTEP plots for 2 and 4, binding studies of L1 and L2 to  $A\beta$  fibrils,  $\text{H}_2\text{O}_2$  production studies by  $A\beta$ -Cu and chelators, cell viability assay for L1, L2, EDTA, and CQ,  $A\beta$  aggregation inhibition studies. This material is available free of charge via the Internet at <http://pubs.acs.org>.

## AUTHOR INFORMATION

### Corresponding Author

\*mirica@wustl.edu

### Notes

The authors declare no competing financial interest.

## ACKNOWLEDGMENTS

We thank the Department of Chemistry at Washington University for startup funds, the Oak Ridge Associated Universities for a Ralph E. Powe Junior Faculty Award to L.M.M., Washington University Knight Alzheimer's Disease Research Center (NIH P50-AG05681) for a pilot research grant to L.M.M., and NIH P30NS69329 to J.K. L.M.M. is a Sloan Fellow.

## REFERENCES

- (1) Annual Report from [www.alz.org](http://www.alz.org): Alzheimer's Disease Facts and Figures.
- (2) Ferri, C. P.; Prince, M.; Brayne, C.; Brodaty, H.; Fratiglioni, L.; Ganguli, M.; Hall, K.; Hasegawa, K.; Hendrie, H.; Huang, Y. Q.; Jorm, A.; Mathers, C.; Menezes, P. R.; Rimmer, E.; Sczufca, M. *Lancet* **2005**, *366*, 2112.
- (3) Jakob-Roetne, R.; Jacobsen, H. *Angew. Chem., Int. Ed.* **2009**, *48*, 3030.
- (4) Perrin, R. J.; Fagan, A. M.; Holtzman, D. M. *Nature* **2009**, *461*, 916.
- (5) LaFerla, F. M.; Green, K. N.; Oddo, S. *Nat. Rev. Neurosci.* **2007**, *8*, 499.

- (6) Roher, A. E.; Lowenson, J. D.; Clarke, S.; Woods, A. S.; Cotter, R. J.; Gowing, E.; Ball, M. J. *Proc. Natl. Acad. Sci. U.S.A.* **1993**, *90*, 10836.
- (7) Jarrett, J. T.; Berger, E. P.; Lansbury, P. T. *Biochemistry* **1993**, *32*, 4693.
- (8) McGowan, E.; et al. *Neuron* **2005**, *47*, 191.
- (9) Kim, J.; Onstead, L.; Randle, S.; Price, R.; Smithson, L.; Zwizinski, C.; Dickson, D. W.; Golde, T.; McGowan, E. *J. Neurosci.* **2007**, *27*, 627.
- (10) Kuperstein, I.; et al. *EMBO J.* **2010**, *29*, 3408.
- (11) Pauwels, K.; Williams, T. L.; Morris, K. L.; Jonckheere, W.; Vandersteen, A.; Kelly, G.; Schymkowitz, J.; Rousseau, F.; Pastore, A.; Serpell, L. C.; Broersen, K. *J. Biol. Chem.* **2012**, *287*, 5650.
- (12) Hardy, J. A.; Higgins, G. A. *Science* **1992**, *256*, 184.
- (13) Hardy, J.; Selkoe, D. J. *Science* **2002**, *297*, 353.
- (14) Lambert, M. P.; Barlow, A. K.; Chromy, B. A.; Edwards, C.; Freed, R.; Liosatos, M.; Morgan, T. E.; Rozovsky, I.; Trommer, B.; Viola, K. L.; Wals, P.; Zhang, C.; Finch, C. E.; Krafft, G. A.; Klein, W. L. *Proc. Natl. Acad. Sci. U.S.A.* **1998**, *95*, 6448.
- (15) Hsia, A. Y.; Masliah, E.; McConlogue, L.; Yu, G.-Q.; Tatsuno, G.; Hu, K.; Kholodenko, D.; Malenka, R. C.; Nicoll, R. A.; Mucke, L. *Proc. Natl. Acad. Sci. U.S.A.* **1999**, *96*, 3228.
- (16) Lesne, S.; Koh, M. T.; Kotilinek, L.; Kaye, R.; Glabe, C. G.; Yang, A.; Gallagher, M.; Ashe, K. H. *Nature* **2006**, *440*, 352.
- (17) Ahmed, M.; Davis, J.; Aucoin, D.; Sato, T.; Ahuja, S.; Aimoto, S.; Elliott, J. I.; Van Nostrand, W. E.; Smith, S. O. *Nat. Struct. Mol. Biol.* **2011**, *17*, 561.
- (18) Gong, Y. S.; Chang, L.; Viola, K. L.; Lacor, P. N.; Lambert, M. P.; Finch, C. E.; Krafft, G. A.; Klein, W. L. *Proc. Natl. Acad. Sci. U.S.A.* **2003**, *100*, 10417.
- (19) Walsh, D. M.; Selkoe, D. J. *J. Neurochem.* **2007**, *101*, 1172.
- (20) Haass, C.; Selkoe, D. J. *Nat. Rev. Mol. Cell Biol.* **2007**, *8*, 101.
- (21) Borutaite, V.; Morkuniene, R.; Valincius, G. *BioMol Concepts* **2011**, *2*, 211.
- (22) Mucke, L. *Nature* **2009**, *461*, 895.
- (23) Lovell, M. A.; Robertson, J. D.; Teesdale, W. J.; Campbell, J. L.; Markesbery, W. R. *J. Neuro. Sci.* **1998**, *158*, 47.
- (24) Barnham, K. J.; Masters, C. L.; Bush, A. I. *Nat. Rev. Drug Discovery* **2004**, *3*, 205.
- (25) Bush, A. I. *Neurobiol. Aging* **2002**, *23*, 1031.
- (26) Faller, P.; Hureau, C. *Dalton Trans.* **2009**, 1080.
- (27) Faller, P. *ChemBioChem* **2009**, *10*, 2837.
- (28) Zatta, P.; Drago, D.; Bolognin, S.; Sensi, S. L. *Trends Pharmacol. Sci.* **2009**, *30*, 346.
- (29) Gaggelli, E.; Kozlowski, H.; Valensin, D.; Valensin, G. *Chem. Rev.* **2006**, *106*, 1995.
- (30) Rauk, A. *Chem. Soc. Rev.* **2009**, *38*, 2698.
- (31) Scott, L. E.; Orvig, C. *Chem. Rev.* **2009**, *109*, 4885.
- (32) Karr, J. W.; Kaupp, L. J.; Szalai, V. A. *J. Am. Chem. Soc.* **2004**, *126*, 13534.
- (33) Cappai, R.; Barnham, K. *Neurochem. Res.* **2008**, *33*, 526.
- (34) Zhu, X.; Su, B.; Wang, X.; Smith, M.; Perry, G. *Cell. Mol. Life Sci.* **2007**, *64*, 2202.
- (35) Hureau, C.; Faller, P. *Biochimie* **2009**, *91*, 1212.
- (36) Molina-Holgado, F.; Hider, R.; Gaeta, A.; Williams, R.; Francis, P. *BioMetals* **2007**, *20*, 639.
- (37) Atwood, C. S.; Moir, R. D.; Huang, X. D.; Scarpa, R. C.; Bacarra, N. M. E.; Romano, D. M.; Hartshorn, M. K.; Tanzi, R. E.; Bush, A. I. *J. Biol. Chem.* **1998**, *273*, 12817.
- (38) Atwood, C. S.; Scarpa, R. C.; Huang, X. D.; Moir, R. D.; Jones, W. D.; Fairlie, D. P.; Tanzi, R. E.; Bush, A. I. *J. Neurochem.* **2000**, *75*, 1219.
- (39) Yoshiike, Y.; Tanemura, K.; Murayama, O.; Akagi, T.; Murayama, M.; Sato, S.; Sun, X. Y.; Tanaka, N.; Takashima, A. *J. Biol. Chem.* **2001**, *276*, 32293.
- (40) Zou, J.; Kajita, K.; Sugimoto, N. *Angew. Chem., Int. Ed.* **2001**, *40*, 2274.
- (41) Tōugu, V.; Karafin, A.; Zovo, K.; Chung, R. S.; Howells, C.; West, A. K.; Palumaa, P. *J. Neurochem.* **2009**, *110*, 1784.
- (42) Bush, A. I. *Curr. Opin. Chem. Biol.* **2000**, *4*, 184.
- (43) Bush, A. I. *Trends Neurosci.* **2003**, *26*, 207.
- (44) Cherny, R. A.; et al. *Neuron* **2001**, *30*, 665.
- (45) Barnham, K. J.; Bush, A. I. *Curr. Opin. Chem. Biol.* **2008**, *12*, 222.
- (46) Cahoon, L. *Nat. Med.* **2009**, *15*, 356.
- (47) Arbiser, J. L.; Kraeft, S.-K.; Van Leeuwen, R.; Hurwitz, S. J.; Selig, M.; Dickerson, G. R.; Flint, A.; Byers, H. R.; Chen, L. B. *Mol. Med.* **1998**, *4*, 665.
- (48) Adlard, P. A.; et al. *Neuron* **2008**, *59*, 43.
- (49) Scott, L. E.; Telpoukhovskaia, M.; Rodriguez-Rodriguez, C.; Merkel, M.; Bowen, M. L.; Page, B. D. G.; Green, D. E.; Storr, T.; Thomas, F.; Allen, D. D.; Lockman, P. R.; Patrick, B. O.; Adam, M. J.; Orvig, C. *Chem. Sci.* **2011**, *2*, 642.
- (50) Perez, L. R.; Franz, K. J. *Dalton Trans.* **2011**, *39*, 2177.
- (51) Hindo, S. S.; Mancino, A. M.; Braymer, J. J.; Liu, Y. H.; Vivekanandan, S.; Ramamoorthy, A.; Lim, M. H. *J. Am. Chem. Soc.* **2009**, *131*, 16663.
- (52) Choi, J.-S.; Braymer, J. J.; Nanga, R. P. R.; Ramamoorthy, A.; Lim, M. H. *Proc. Natl. Acad. Sci. U.S.A.* **2010**, *107*, 21990.
- (53) Zhang, Y.; Chen, L.-Y.; Yin, W.-X.; Yin, J.; Zhang, S.-B.; Liu, C.-L. *Dalton Trans.* **2011**, *40*, 4830.
- (54) Dedeoglu, A.; Cormier, K.; Payton, S.; Tseitlin, K. A.; Kremisky, J. N.; Lai, L.; Li, X. H.; Moir, R. D.; Tanzi, R. E.; Bush, A. I.; Kowall, N. W.; Rogers, J. T.; Huang, X. D. *Exp. Gerontol.* **2004**, *39*, 1641.
- (55) Hureau, C.; Sasaki, I.; Gras, E.; Faller, P. *ChemBioChem* **2010**, *11*, 950.
- (56) Choi, J.-S.; Braymer, J. J.; Park, S. K.; Mustafa, S.; Chae, J.; Lim, M. H. *Metallomics* **2011**, *3*, 284.
- (57) Rodriguez-Rodriguez, C.; de Groot, N. S.; Rimola, A.; Alvarez-Larena, A.; Lloveras, V.; Vidal-Gancedo, J.; Ventura, S.; Vendrell, J.; Sodupe, M.; Gonzalez-Duarte, P. *J. Am. Chem. Soc.* **2009**, *131*, 1436.
- (58) Braymer, J. J.; DeToma, A. S.; Choi, J.-S.; Ko, K. S.; Lim, M. H. *Int. J. Alzheimers Dis.* **2011**, *2011*, 623051.
- (59) Necula, M.; Kaye, R.; Milton, S.; Glabe, C. G. *J. Biol. Chem.* **2007**, *282*, 10311.
- (60) Evans, D. F. *J. Chem. Soc.* **1959**, 2003.
- (61) De Buysser, K.; Herman, G. G.; Bruneel, E.; Hoste, S.; Van Driessche, I. *Chem. Phys.* **2005**, *315*, 286.
- (62) Mashraqui, S. H.; Kumar, S.; Vashi, D. *J. Inclusion Phenom. Macro.* **2004**, *48*, 125.
- (63) Bruker Analytical X-Ray, Madison, WI, 2008.
- (64) Sheldrick, G. M. *Acta Cryst.* **2008**, *A64*, 112.
- (65) Gans, P.; Sabatini, A.; Vacca, A. *Ann. Chim.* **1999**, 45.
- (66) Alderighi, L. *Coord. Chem. Rev.* **1999**, *184*, 311.
- (67) Klein, W. L. *Neurochem. Int.* **2002**, *41*, 345.
- (68) Himes, R. A.; Park, G. Y.; Siluvai, G. S.; Blackburn, N. J.; Karlin, K. D. *Angew. Chem., Int. Ed.* **2008**, *47*, 9084.
- (69) Mohanty, J. G.; Jaffe, J. S.; Schulman, E. S.; Raible, D. G. *J. Immunol. Meth.* **1997**, *202*, 133.
- (70) Zhou, M.; Diwu, Z.; Panchuk-Voloshina, N.; Haugland, R. P. *Anal. Biochem.* **1997**, *253*, 162.
- (71) Richer, S. C.; Ford, W. C. L. *Mol. Hum. Reprod.* **2001**, *7*, 237.
- (72) Votyakova, T. V.; Reynolds, I. J. *J. Neurochem.* **2001**, *79*, 266.
- (73) Dickens, M. G.; Franz, K. J. *ChemBioChem* **2010**, *11*, 59.
- (74) Folk, D. S.; Franz, K. J. *J. Am. Chem. Soc.* **2010**, *132*, 4994.
- (75) Nolan, E. M.; Lippard, S. J. *Acc. Chem. Res.* **2008**, *42*, 193.
- (76) Tomat, E.; Lippard, S. J. *Curr. Opin. Chem. Biol.* **2010**, *14*, 225.
- (77) Lipinski, C. A.; Lombardo, F.; Dominy, B. W.; Feeney, P. J. *Adv. Drug Delivery Rev.* **2001**, *46*, 3.
- (78) Storr, T.; Merkel, M.; Song-Zhao, G. X.; Scott, L. E.; Green, D. E.; Bowen, M. L.; Thompson, K. H.; Patrick, B. O.; Schugar, H. J.; Orvig, C. *J. Am. Chem. Soc.* **2007**, *129*, 7453.
- (79) Perrin, D. D. *Dissociation constants of organic bases in aqueous solution*; Butterworths: London, 1972.
- (80) Martell, A. E.; Smith, R. M. *Critical Stability Constants*; Plenum: New York, 1976; Vol. IV.
- (81) Danielsson, J.; Pierattelli, R.; Banci, L.; Gräslund, A. *FEBS J.* **2007**, *274*, 46.
- (82) Hou, L.; Zagorski, M. G. *J. Am. Chem. Soc.* **2006**, *128*, 9260.
- (83) Huang, C. Y. *Methods Enzymol.* **1982**, *87*, 509.

- (84) Addison, A. W.; Rao, T. N.; Reedijk, J.; van Rijn, J.; Verschoor, G. C. *J. Chem. Soc., Dalton Trans.* **1984**, 1349.
- (85) Klunk, W. E.; Wang, Y. M.; Huang, G. F.; Debnath, M. L.; Holt, D. P.; Mathis, C. A. *Life Sci.* **2001**, *69*, 1471.
- (86) Lockhart, A.; Ye, L.; Judd, D. B.; Merritt, A. T.; Lowe, P. N.; Morgenstern, J. L.; Hong, G. Z.; Gee, A. D.; Brown, J. *J. Biol. Chem.* **2005**, *280*, 7677.
- (87) Yona, R. L.; Mazeris, S.; Faller, P.; Gras, E. *ChemMedChem* **2008**, *3*, 63.
- (88) Reinke, A. A.; Seh, H. Y.; Gestwicki, J. E. *Bioorg. Med. Chem. Lett.* **2009**, *19*, 4952.
- (89) Only one other study reports the A $\beta$ -binding affinity of rhenium complexes of 2-phenylbenzothiazole derivatives: Lin, K. S.; Debnath, M. L.; Mathis, C. A.; Klunk, W. E. *Bioorg. Med. Chem. Lett.* **2009**, *19*, 2258.
- (90) Garai, K.; Sahoo, B.; Kaushalya, S. K.; Desai, R.; Maiti, S. *Biochemistry* **2007**, *46*, 10655.
- (91) Tew, D. J.; Bottomley, S. P.; Smith, D. P.; Ciccotosto, G. D.; Babon, J.; Hinds, M. G.; Masters, C. L.; Cappai, R.; Barnham, K. J. *Biophys. J.* **2008**, *94*, 2752.
- (92) Dahlgren, K. N.; Manelli, A. M.; Stine, W. B.; Baker, L. K.; Krafft, G. A.; LaDu, M. J. *J. Biol. Chem.* **2002**, *277*, 32046.
- (93) Stine, W. B.; Dahlgren, K. N.; Krafft, G. A.; LaDu, M. J. *J. Biol. Chem.* **2003**, *278*, 11612.
- (94) Huang, X. D.; et al. *J. Biol. Chem.* **1999**, *274*, 37111.
- (95) Wogulis, M.; Wright, S.; Cunningham, D.; Chilcote, T.; Powell, K.; Rydel, R. E. *J. Neurosci.* **2005**, *25*, 1071.
- (96) Stine, B. W.; Jungbauer, L.; Yu, C.; LaDu, M. J. *Met. Mol. Biol.* **2010**, *670*, 13.
- (97) The inhibition of A $\beta$ <sub>42</sub> aggregation in presence of 2  $\mu$ M and 10  $\mu$ M of L1 or L2 was also investigated by TEM and Western blotting and gave similar results (Figures S27 and S28, Supporting Information).
- (98) Mancino, A. M.; Hindo, S. S.; Kochi, A.; Lim, M. H. *Inorg. Chem.* **2009**, *48*, 9596.
- (99) Murray, M. M.; Bernstein, S. L.; Nyugen, V.; Condron, M. M.; Teplov, D. B.; Bowers, M. T. *J. Am. Chem. Soc.* **2009**, *131*, 6316.
- (100) Yan, Y.; Wang, C. *J. Mol. Biol.* **2007**, *369*, 909.
- (101) A recent study reports a bifunctional compound that leads to increased metal-based A $\beta$ <sub>40</sub> neurotoxicity, although the formation of soluble A $\beta$  oligomers was not unambiguously demonstrated (ref 53).